https://doi.org/10.26682/sjuod.2022.25.2.36
Journal of University of Duhok., Vol. 25, No.2(Pure and Engineering Sciences), Pp 389-403, 2022

PHOTOGRAMMETRIC MODELLING OF STREET CONDITIONS USING A VEHICLE-MOUNTED NON-METRIC CAMERA

ALENA **F**UAD **T**OMA[*] and **R**AAD **A**WAD **K**ATTAN[**]
[*]Dept. of Civil Engineering, College of Engineering, University of Duhok, Kurdistan Region-Iraq
[**]Dept. of Surveying Engineering, College of Engineering, University of Duhok, Kurdistan Region-Iraq

(Received: September 7, 2022; Accepted for Publication: November 21, 2022)

ABSTRACT

Monitoring and modeling pavement distresses can employ either simple methods like direct measurements by tapes or straight edges, or more sophisticated approaches like laser scanners and stereoscopic cameras held at the ends of fixed poles.

This study aims to detect pavement distress's shape and position, such as cracks. For this purpose, overlapped images were collected for the distressed area to obtain complete coverage of the street conditions located in front of the College of Engineering /University of Duhok. Kurdistan Region, Iraq. A single non-metric camera attached to the side and the front of the vehicle is the approach employed as an image-collecting device. The camera shutter speed is selected to have a sequence of overlapped images to be processed, producing the pavement surface orthomosaic.

The plane of the image in this study is inclined or obliquely relative to the pavement surface, so a gap is expected in the overlap area in the near range. To overcome this drawback and other problems, an indoor grid and tiles test was conducted to obtain the required parameters such as focal length, overlap percentage, camera shutter speed, and vehicle speed.

Ground control points (GCPs) and checkpoints for processing and accuracy checks were provided in each test and distributed evenly in the model area.

The indoor parameter collecting tests revealed that the Root Mean Square Error (RMSE) for the (15) checkpoints was ±0.013m in X and ±0.016m in Y coordinates. Using a larger tilt angle and increasing camera height gave a root mean square error of ±0.009m in X and ±0.013m in Y, respectively.

Image processing was conducted using Agisoft PhotoScan as it provided adequate accuracy and modeling tools in several previous papers.

KEYWORD: Non-metric camera, Close-range photogrammetry, Ground control points, Distresses, Focal length, Convergent Photos

1. INTRODUCTION

Asphalt surface roads are the major transportation means in most of the world's countries. However, due to surface aging, heavy traffic loads, design and construction problems, and weather conditions, different types of distress are expected to occur on these surfaces. Moreover, maintaining these surfaces consumes a high percentage of the country's budget. Therefore, an efficient observation and maintenance scheme is essential to reduce maintenance costs and effort.

The techniques for monitoring street distortions range from simple to more complicated techniques. The simple techniques are manual methods that use simple tools such as the level bar or straight edge. In contrast, various complicated techniques include Profilographs, 3-D laser scanners, automated image-based crack detection systems, and photogrammetric techniques (Knyaz & Chibunichev, 2016).

The approach implemented in this study is digital close-range photogrammetry (DCRP). It is considered a fast data collection method with available resources, and it can record street conditions for any intended future maintenance (Fawzy, Basha, & Botross, 2020).

This research aims are to detect the distresses, particularly cracks in the road pavements, using a vehicle-mounted non-metric camera, to obtain a three-dimensional model or an orthomosaic with positioned coordinates, and, finally, to obtain a unified record that contains cracks' positions and lengths that will assist later in any intended street's maintenance.

In this research, overlapping oblique images were captured via a non-metric camera, the Nikon D5300, mounted on a vehicle in two different positions: the side position and the front position.

An indoor preliminary test utilizing plastic mesh and tiles was conducted first to obtain the needed imaging parameters such as tilt angle, camera base, overlap, and shutter speed. The results of these tests were then implemented on the front and side position imaging series and were collected later.

The images were processed using Agisoft PhotoScan to build a three-dimensional point cloud and orthomosaic (Cross, Farhadmanesh, & Rashidi, 2020). In addition, ground control points (GCPs) were measured for each case to be included in the processing stages.

2. RELATED WORK

On the advanced side of pavement condition techniques, 3D laser scanners and close-range photogrammetry are used for pavement monitoring.

2.1 3D Laser Scanner

Terrestrial laser scanning (TLS) is a technique that works by emitting laser pulses toward the required surface area and results in the acquisition of a georeferenced model of the surface texture. This technique requires a continuous ground position measurement. Thus, a GPS is attached to the device the whole time, thus obtaining the XYZ coordinates of various points on the ground (Lee, 2001) (Vosselman & Maas, 2010).

Figure (1) shows one of the laser scanner devices, Mandli's LiDAR Vehicle (Cross et al., 2020).

Fig. (1) Mandli's Mobile LiDAR Vehicle (Cross et al., 2020)

2.2 Photogrammetric Methods

The photogrammetric methods, generate a 3D model and recreate objects' textures, which are considered cheap since they can use consumer-grade cameras with affordable lenses. They can also be held at changeable distances by controlling the lenses, focal lengths, and changeable exposure distances.

Ahmed, Haas, and Haas (2011) employed the photogrammetric technique in pavement monitoring. The camera was freely titled with positions that were not standard spatially. The flash was used in natural daylight and, the camera height was between (1.5-1.6) m above the surface of the street. The exposure stations were randomly chosen to sustain a fixed overlap, while the distance between the camera and the surface of the ground was not fixed and ranged between (2-7 or 10) m due to the tilt of the camera and the ray angle that passed through each point and the lenses.

This research, showed that the camera was stationary, so no time or speed was specified. Figure (2) shows the resultant zoomed-in part of the produced point clouds.

Fig. (2) A zoomed-in part of point clouds (Ahmed et al., 2011)

Kattan, Abdulrahman, Gilyana, and Zaya (2021) used photogrammetric techniques to create a 3-D virtual model of the College of Engineering/University of Duhok in the Kurdistan Region of Iraq, using vertical and oblique images from a UAV and control points from a GPS RKT system and a reflectorless total station.

This study employed Agisoft PhotoScan, the Global Mapper, and Recap software to generate a 3-D model, a digital elevation model, and an orthomosaic.

According to Kattan et al. (2021), the Leica Viva GNSS, GS10 base receiver, and GS15 rover receiver were used to set 9 control points on the ground surrounding the building as positions to employ the Leica TCR1101 total station in a reflectless mode to measure about 92 points on the building's façade, while the rover GS15 receiver was used to measure 27 points on the building's roof surface. The GCPs were in WGS 84 / UTM zone 38N coordinate system.

The Phantom 4 Pro, 4K- DJI was used for the imaging process in four flights; two were oblique and the others were vertical. The Agisoft PhotoScan was to process the resulting 183 images and 128 ground control points. Distance measurements had a relative accuracy of 0.72% to 4.92%, with a maximum standard deviation of 4 cm.

Figures (3) a and b show the tiled model resulting from Agisoft PhotoScan and the model with the control points.

Fig. (3): a- The tiled model from Agisoft PhotoScan **b-** The model with control points (Kattan et al., 2021).

Abdulrahman, Kattan, and GILYANA (2020) used a DJI Phantom 4 Pro drone to create an orthophoto and compare their accuracy to the accuracy of the already existing orthophoto created from an aerial survey carried out by Vossing German Company in Duhok city in 2011 employing a reference base of GPS ground control points.

265 photos of the University of Duhok Campus College of Engineering, Duhok city, Kurdistan region/ Iraq were captured within 11 flight path lines in the South-East to North-West direction, with front and side overlap coverage of 70% and 40%, respectively. 19 GCPs were measured by GPS-RTK in the WGS84- 38N coordinate system; 9 of them were used for the DEM and orthomosaic processing, and the remaining 12 were used as checkpoints.

According to Abdulrahman et al. (2020), the digital elevation model (DEM) was used as a base for the orthophotos. The Agisoft PhotoScan and Pix4D Mapper software were employed for data processing and analysis. An accuracy of sub-centimeters was achieved from the UAV orthophoto at low flight altitudes for horizontal positions.

Figures (4) a and b show the DEM and the orthomosaic obtained from the Agisoft PhotoScan respectively, the orthomosaic was later exported in TIFF form and used in AutoCAD Civil 3D to create the final orthomosaic.

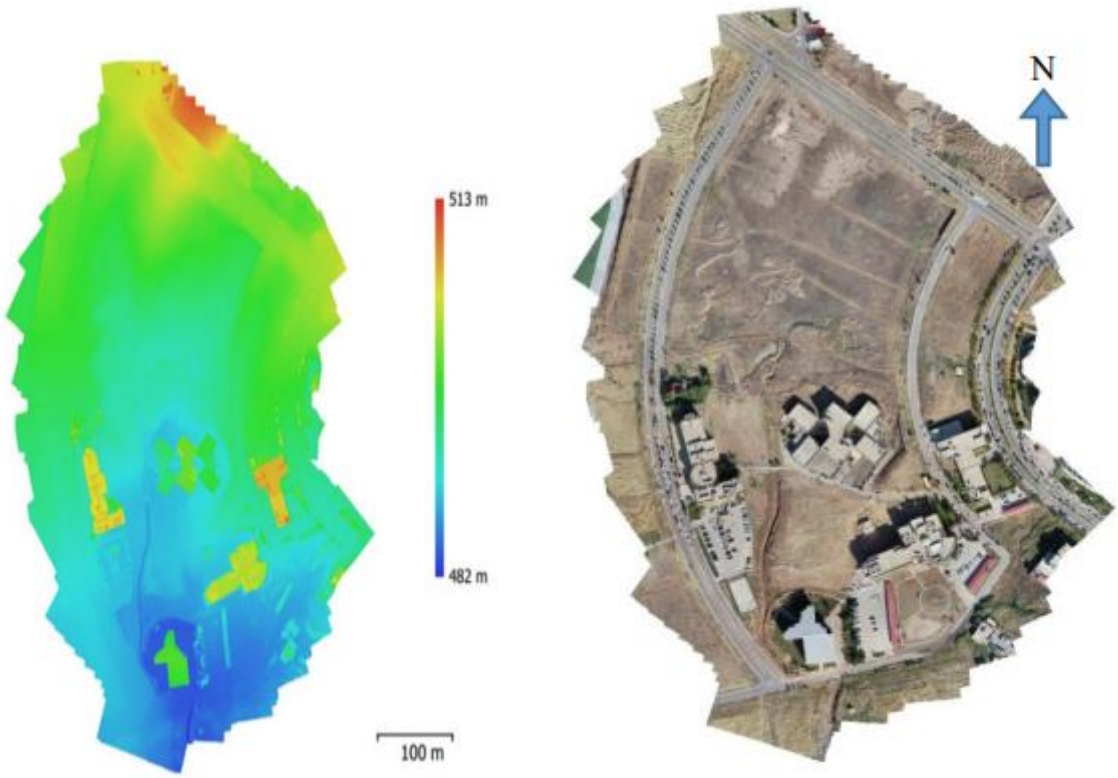

Fig. (4): a- The digital elevation model **b-** The orthomosaic (Abdulrahman et al., 2020).

3. METHDOLOGY

3.1 Photogrammetric Ground Control points

For the purpose of georeferencing the photogrammetric model, ground control points in the feature space have to be located and measured in the required area. The number and distribution of these GCPs are of vital importance for the accuracy of the whole process.

All the points in the field are employed as some type of control points, but about 80% of the points are typically used as GCPs for reconstruction purposes, while the remaining 20% are used as checkpoints. In the absence of measured GCPs, an error might appear in the scale or the orientation of the imagery reconstruction in addition to incorrect absolute position information (Wolf, 2021).

Wolf (2021) showed that when less than 5 GCPs are used, the amount of orthophotos error increases rapidly; while using more than 5 GCPs results in more accurate digital elevation model results but relatively minor accurate overall results.

Yu, Kim, Lee, and Son (2020) stated that 12 GCPs were important for the overall accuracy in small and medium sites while the GCPs' spatial distribution across the area is also vital.

Other studies showed that in order to minimize the planimetry errors, some GCPs should be placed around the edges of the targeted area, while to minimize the altimetry errors, a stratified distribution with some GCPs must be applied inside the targeted area (Martínez-Carricondo et al., 2018).

In this study, the number of the distributed GCPs was chosen to be enough, uniform, and, according to the photogrammetric theories, as much as possible to cover the entire model area, while in some places it might be limited depending on the road condition. The approach used in GCPs measuring was by directly taping the location of the GCPs.

In this research, some of the measured control points were kept for the later accuracy assessment of the whole process as checkpoints.

3.2 The Non-Metric Camera

Nonmetric cameras have uncalibrated and possibly unstable interior orientation elements and no fiducial marks. Challenges are introduced by using non-metric cameras with changeful and zoom lenses and are more challenging for meaningful engineering projects due to the changed interior orientation elements throughout

the zoom range (Ahmed et al., 2011). This drawback can be compensated for by using efficient self-calibrating bundle adjustment included in the processing software.

In this research, a Nikon D5300 camera was attached to a vehicle with an attachment device shown in figure (3).

Fig. (3): The Nikon D5300 with the attachment apparatus

According to the manufacturer, the camera specifications are:

- Type: Single-lens reflex digital camera
- Lens mount: Nikon F mount (with AF contacts)
- Effective angle of view: Nikon DX format; focal length equivalent to approximately 1.5x that of lenses with FX format angle of view.
- Effective pixels: 24.2 million
- Focal length ranges from 18 to 55 mm
- Image sensor: 23.5 x 15.6 mm CMOS sensor
- Total pixels: 24.78 million
- Image size (pixels): 6000 x 4000 (L), 4496 x 3000 (M), 2992 x 2000 (S)
- Viewfinder: Eye-level pentamirror single-lens reflex viewfinder
- Lens aperture: Instant return, electronically controlled.
- Shutter type: Electronically controlled vertical-travel focal-plane shutter with 1/4000 to 30 s in steps of 1/3 or 1/2 EV, bulb, time.

Since this camera is a non- metric one, its internal parameters such as focal length, symmetric radial and decentering lens distortion, and principal point location are unknown, this will be overcome by applying the embedded self-calibration bundle adjustment in the used software.

3.3 Image Processing

Image processing was conducted using Agisoft PhotoScan, a stand-alone software product that conducts photogrammetric procedures on digital photos and creates three-dimensional spatial data.

The software requires overlapped vertical or oblique images with sufficient ground control points. The final output utilized in this study is the distressed area orthomosaic.

Three tests were conducted in this study, all aiming for the same results which is a 3-D orthomosaic model with the same procedures, the only differences were the number of images and the number of ground control points required for each test depending on the test's conditions.

The first test was the grid and tiles indoor test which included 12 images and 15 GCPs the second test was the side-looking mobile camera test which included 44 images and 8 GCPs, and the final test was the front-looking mobile camera test which included 35 images and 14 GCPs.

The Agisoft PhotoScan software sequence for all of the tests is shown in figure (4).

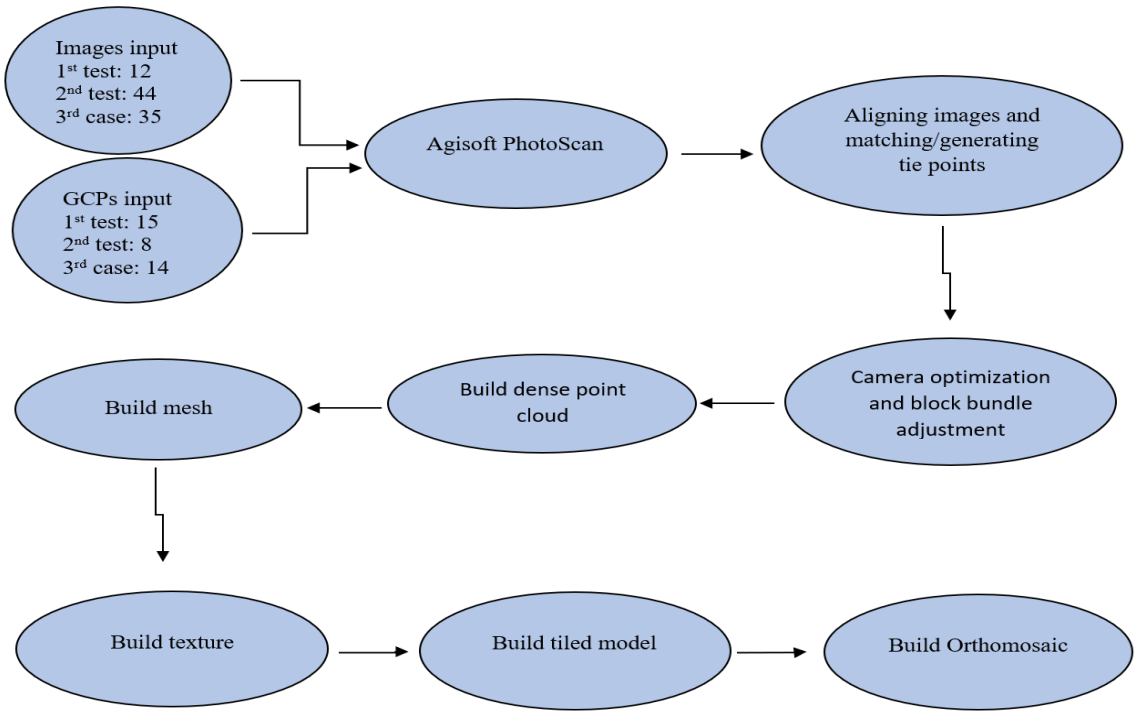

Fig. (4): Agisoft PhotoScan sequence.

4. TESTS AND RESULTS

Initial imaging and modeling tests revealed gaps in the near-range overlapped area. The reason for the gap is the variation of the object depth from a short-range having small coverage to an extensive range with broader coverage, figure (5).

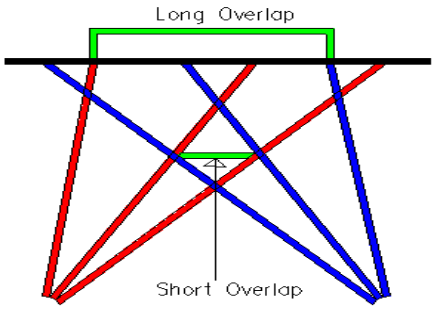

Fig. (5): The variation in the overlapped area with different depths

To overcome this issue, an initial indoor test made using a plastic grid and tiles was conducted to obtain parameters such as the appropriate convergent angle, tilt angle, and speed of the camera and vehicle.

Depending on this initial test, pavement distress model tests were conducted with the camera attached either to the side or to the front of the vehicle.

5.1 Indoor grid and tiles model test

A (6x5) m plastic mesh was laid on the ground with several (50x50) cm tiles distributed over it. This grid mesh served as a controlled site to simulate street conditions and to decide imaging parameters such as:

a. Focal length (f)

The focal length depends on the type of camera used, the object distance, and its

consistency with the other needed parameters to ensure sufficient overlap and coverage. In this study, the focal length was selected between 18 to 24 mm.

b. Convergent angle (φ)

To ensure comprehensive ground coverage and increase the distance between exposure stations, the camera axis was inclined to the object space by a convergent angle (φ). In addition, to ensure stereoscopic ground coverage, left-to-right and right-to-left passes were essential, figure (6).

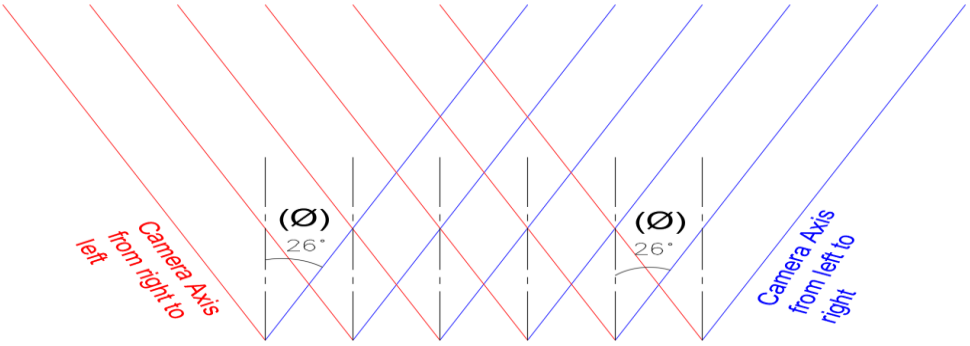

Fig. (6): The convergent angle (φ) with which the camera axis is tilted from the vertical axis.

c. Tilt angle (t)

The tilt angle is the angle of inclination of the camera axis from the nadir. In this study, the tilt angle was always downward between 95° to 115°, figure (7-a).

d. Photo coverage (w)

Photo ground coverage depends on the focal length, sensor size, and object distance, figure (7-b).

For a (6) m object distance, (18) mm focal length, and sensor width of (23.5) mm, the ground coverage will be:

$$\frac{18}{23.5} = \frac{6/\cos 26^\circ}{w}$$ therefore, w= 8.7 m

This coverage will increase as the camera axis is not normal to the object space and depends on the convergent angle. If the convergent angle is 26°, then the photo coverage (G) will equal to

$$\frac{8.7}{\cos 26^\circ} = 9.7 \text{ m}$$

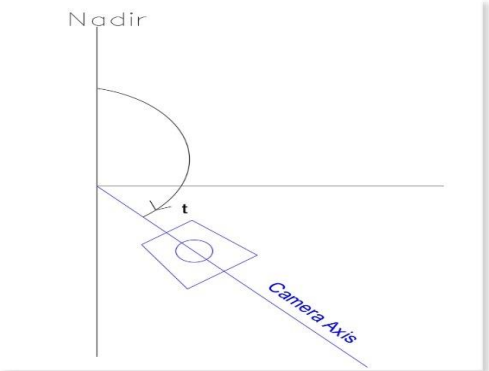

Fig. (7): a- Tilt angle

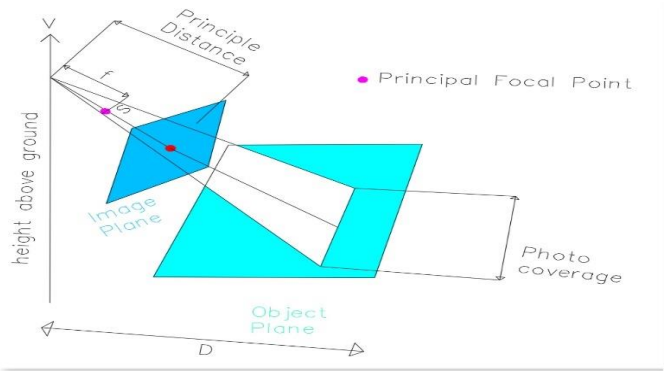

b- Photo coverage

e. Distance between exposure stations (image base) (B)

The image base value decides the number of required images and the overlap value. To ensure the best geometrical intersection accuracy, the base/depth ratio should be 1 to 2. For higher base/depth ratios, a complete overlap in the near range is impossible, as in the case of the present study.

f. Overlap

Overlap value = (G-B)/G

Where G is the coverage, and B is the distance between the exposure stations (Roberts et al., 2019).

g. Camera height

The camera height was selected depending on the available position of the camera mount on the vehicle. The higher the camera position, the better the camera height was set at 1.35 to 2.0 m.

h. Time between exposures

The time set between the consecutive images should be in harmony with the distance between camera positions and the vehicle's speed.

For a vehicle speed of 5km/h (1.4 m/sec) and a distance between exposures (B) of 1m, then

Time = $\frac{1}{1.4}$ = 0.7 sec

After many practical and mathematical experiments, the parameters of this test were conveniently set to be:

Maximum object distance=6 m
Focal length=24 mm
Convergent angle=26°
Maximum photo coverage =7.28 m
Overlap value =86%
Tilt angles= 110° and 115°
Camera heights =1.5 m and 2 m

In this indoor test, (15) GCPs and (20) check points were measured on the ground model for georeferencing purposes. In addition, a local coordinate system was assigned. To ensure verticality, the coordinates were measured manually using tape and a large-sized right-angled triangle explicitly manufactured for this purpose.

The points were spread throughout the model, specified by colored stickers with a pen-drawn crack shape to mimic reality. The point of origin (0,0,0) was located on the down, left end of the model to ensure positive coordinates for all points.

The Z coordinates for all points =0.00m except for two points marked with warning triangles of 0.25m height.

Figures (8) a and b show the control points of the model marked using green stickers, and the check points marked with white stickers, along with a zoomed-in image of the targets.

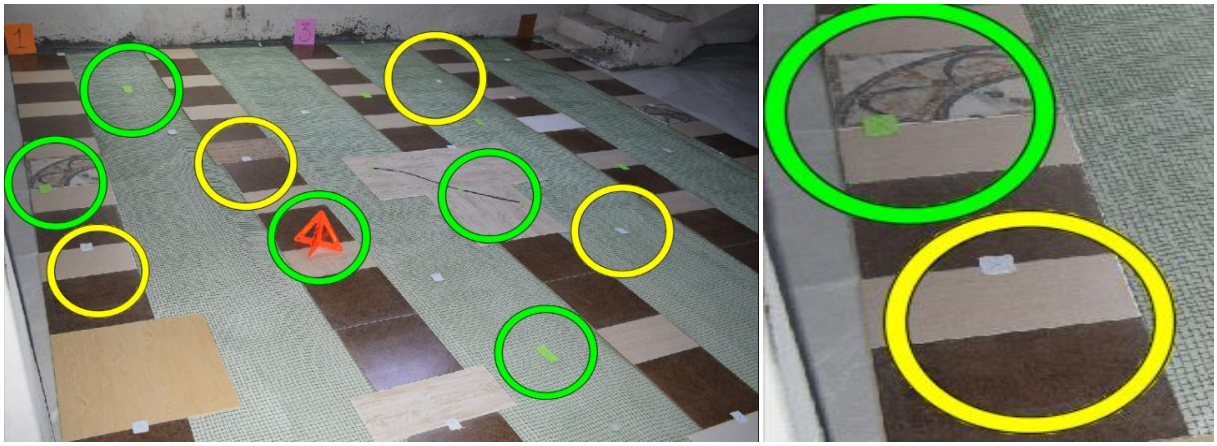

Fig. (8): a-GCPs (green) and Check points (white) of the created model **b**- A zoomed-in GCPs

The checkpoints were measured again on the orthomosaic model extracted from the Agisoft PhotoScan. The error in each coordinate is the difference between the directly measured coordinates and the Agisoft orthomosaic coordinates.

The error in X (e_X=Xi-$\hat{Xi}$),
The error in Y (e_Y=Yi-$\hat{Yi}$)

The Root Mean Square Error (RMSE) for each coordinate is:

RMSE = $\sqrt{\frac{\sum_{i=1}^{n}(Xi-\hat{Xi})^2}{n}}$

Where n is the number of checkpoints.

Figure (9) shows the arrangement of the test model, including the positions of control points and check points.

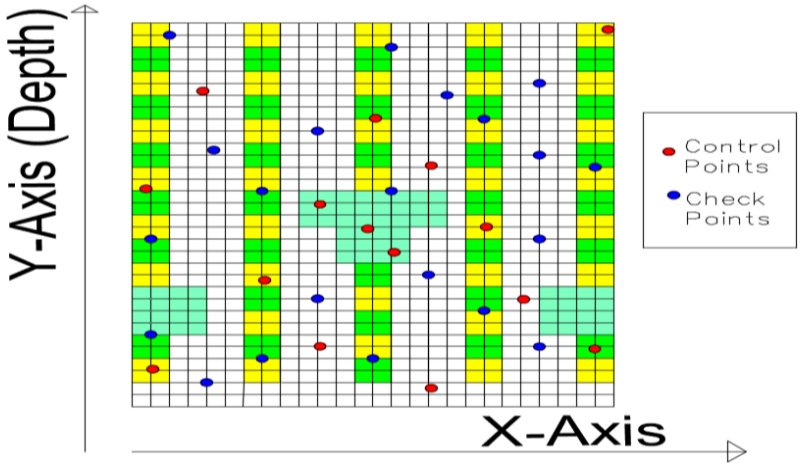

Fig. (9): Grid and tiles model test details

The orthomosaic models for two test cases of this test are shown in figure (10). The first utilized a (110º) tilt angle and a (1.5) m camera height. The second utilized a (115º) tilt angle and a (2) m camera height.

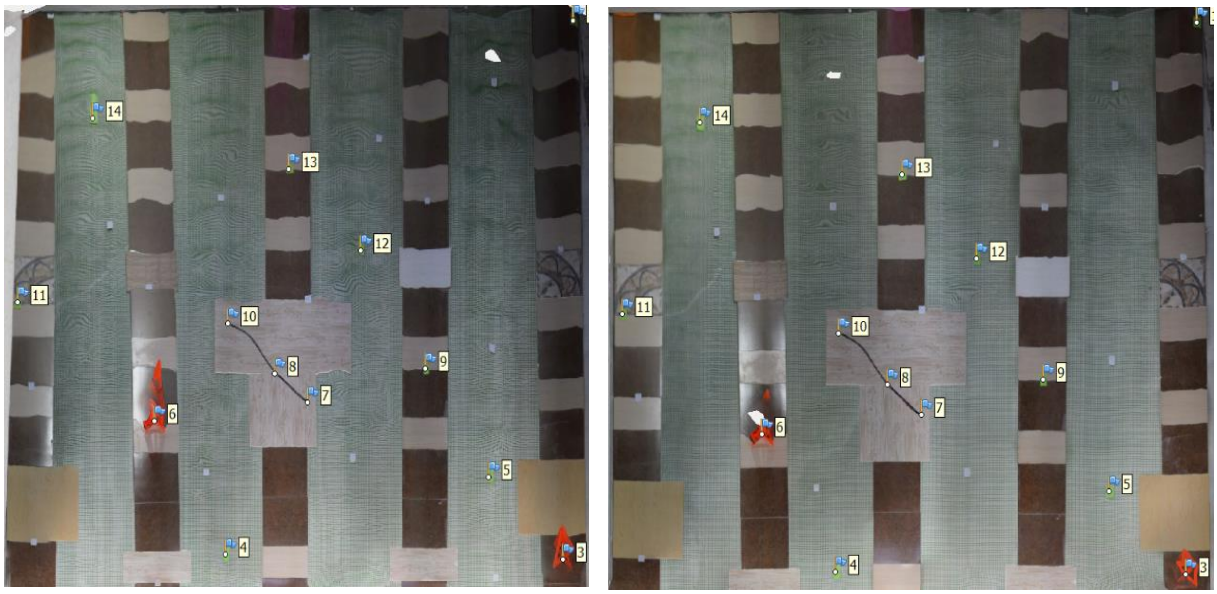

Fig.(10): a- Grid and Tiles experiment Orthomosaic with 110º tilt angle b- Grid and Tiles experiment Orthomosaic with 115º tilt angle

Table (1) shows the coordinates of the 15 points directly measured using the orthomosaic models plus the error values and RMSE.

Table (1): Accuracy check for grid and tiles test

	Directly measured coordinates (m)		Model coordinates at 110º tilt angle and 1.5 m height (m)		Discrepancies at 110º tilt angle and 1.5 m height (m)		Model coordinates at 115º tilt angle and 2 m height (m)		Discrepancies at 115º tilt angle and 2 m height (m)	
Point	X	Y	X	Y	e_X	e_Y	X	Y	e_X	e_Y
1	0.255	1.86	0.216	1.823	0.039	0.037	0.238	1.83	0.017	0.03
2	1.73	2.395	1.73	2.385	0	0.01	1.721	2.385	0.009	0.01
3	3	2.505	3.008	2.504	0.008	0.001	3.003	2.504	0.003	0.001
4	0.225	3.11	0.195	3.082	0.03	0.028	0.214	3.09	0.011	0.02
5	4.223	3.375	4.23	3.389	0.007	0.014	4.231	3.38	0.008	0.005
6	2.613	3.785	2.618	3.78	0.005	0.005	2.619	3.781	0.006	0.004
7	1.22	3.885	1.225	3.878	0.005	0.007	1.222	3.88	0.002	0.005
8	4.828	4.18	4.836	4.196	0.008	0.016	4.841	4.197	0.013	0.017
9	0.885	4.395	0.881	4.379	0.004	0.016	0.881	4.381	0.004	0.014
10	3.66	4.579	3.662	4.584	0.002	0.005	3.667	4.582	0.007	0.003
11	1.86	4.588	1.859	4.602	0.001	0.014	1.86	4.583	0	0.005
12	3.24	5.068	3.239	5.076	0.001	0.008	3.246	5.071	0.006	0.003
13	4.244	5.515	4.249	5.536	0.005	0.021	4.258	5.529	0.014	0.014
14	2.605	5.74	2.606	5.74	0.001	0	2.615	5.745	0.01	0.005
15	0.371	6.084	0.365	6.069	0.006	0.015	0.375	6.067	0.004	0.017
				RMSE of X = 0.013m RMSE of Y = 0.016m				RMSE of X = 0.009m RMSE of Y = 0.013m		

Figure (11) shows a graphical representation of these errors with points' depth.

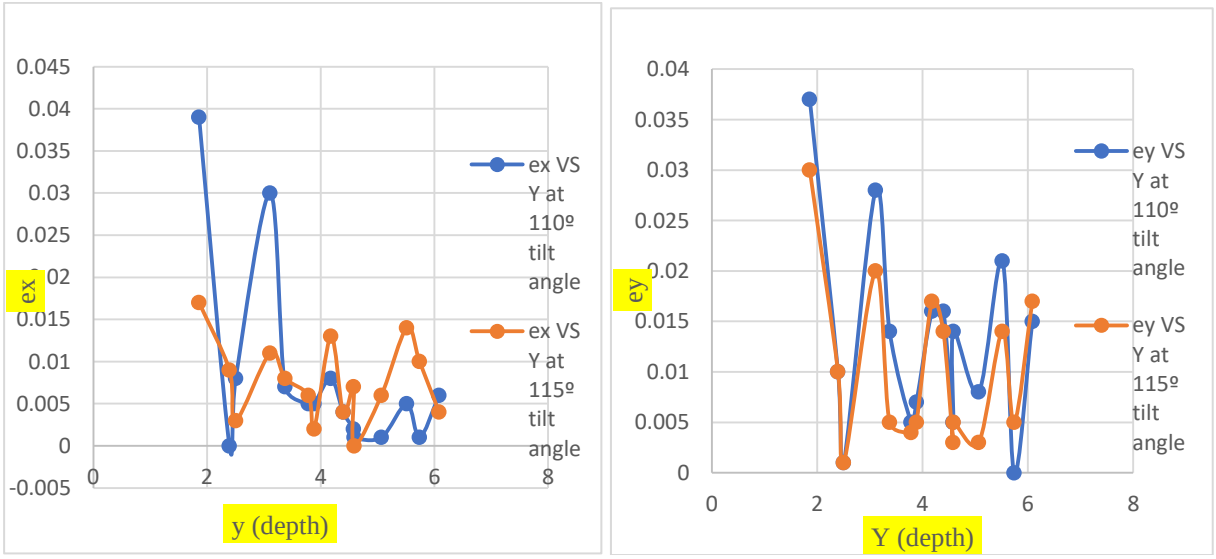

Fig. (11): Check points coordinates versus depth of grid and tiles test

From the table and the figures, one can conclude that the model measured errors were in the range of 3 to 4 cm as maximum values for both cases. A remarkable reduction in errors is noticed heading from the near range to the far range. A slight errors reduction was also noticed using a higher camera height and a larger tilt angle.

5.2 street conditions via side position camera

To model the pavement condition of a street within the university of Duhok campus, the Nikon D5300 attached to the side window of a vehicle, as shown in figure (12-a), was used.

The imaging parameters selected were (6) m object distance, (24) mm Fl, (26º) convergent angle, and (1) m distance between exposure stations, which made the photo coverage equal to (7.28) m, and the overlap remained more than (86) %, a (1.35) m camera height from the ground, (110º) downwards tilt angle, (1) sec shutter time, and (3 - 4) km/h vehicle speed.

To obtain a stereoscopic coverage of the pavement surface and due to the lack of stereometric cameras held at the end of a fixed bar, also to avoid rotating the camera after each exposure, two imaging passes were carried out, one from left to right and the camera axis looking right. The other pass from right to left, and the camera axis looks left.

Figure (12-b) shows the images collected in two passes, from left to right and then from right to left.

Fig. (12): a- The camera attached to the vehicle's side window **b-** Images captured in two passes, right to left and left to right

Eight local control points were well distributed on the pavement surface, and curbstone was marked and measured. The point of origin was selected to ensure all positive coordinates, figure (13).

Fig. (13): GCP (black and blue sticker) with the origin point (warning triangle)

The Orthomosaic obtained using the Agisoft PhotoScan is shown in figure (14-a), and a zoomed-in view of the cracked area is in figure (14-b).

Fig. (14): a-Orthomosaic of the street distresses obtained from a side position camera **b-**A zoomed-in view of the crack section

5.3 Street conditions via front position camera

A front-looking camera position was tested as an alternative to the side-looking camera coverage. The overlap will be ensured by having consecutive images of the same spot collected during the vehicle's forward movement.

A selected street was imaged with the camera attached to the vehicle's hood at the height of (1.45) m and a tilt angle of about (95º) downwards, with a shutter time of (1) sec. The vehicle's speed was (5) km/h, figures (15) a and b.

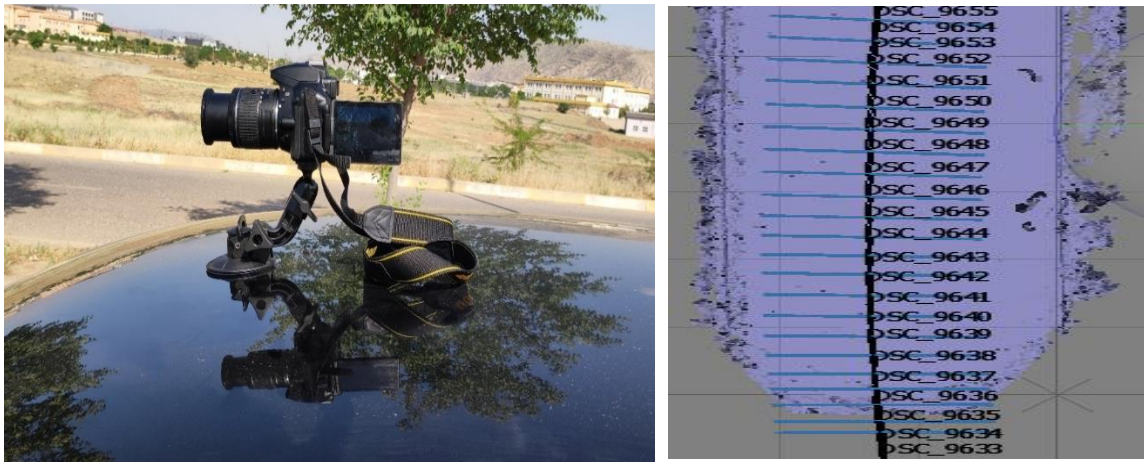

Fig. (15) a- Camera attached to the vehicle's hood **b-** Consecutive images taken in a direction of the vehicle motion

(14) local control points and (4) local checkpoints were spread along the street. The reference point (0,0,0) was located on the downright end of the street, which made the x coordinates negative and the y coordinates positive. The stickers marking the GCPs with the zoom-in GCPs and the checkpoints are shown in figures (16) a, b, and c, respectively.

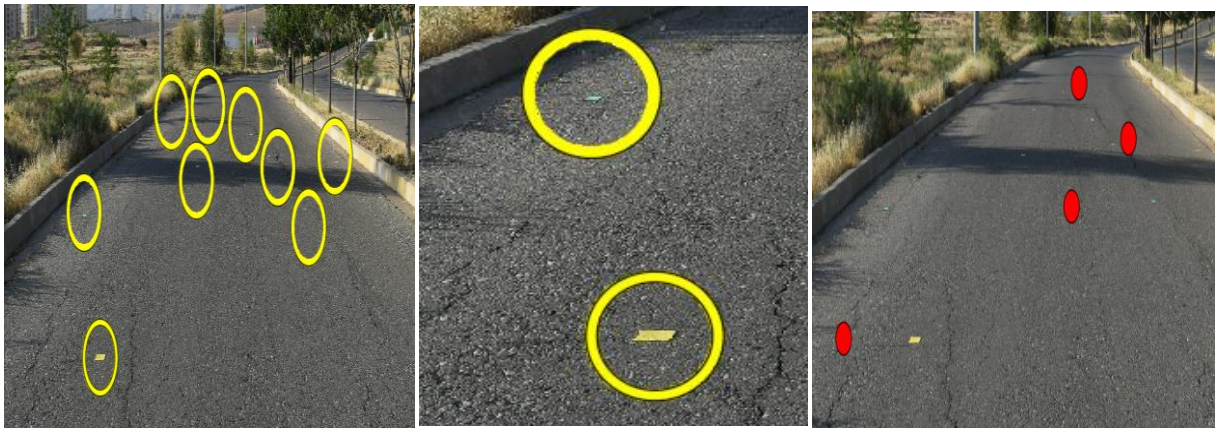

Fig. (16): a- GCPs **b-**A zoomed-in GCPs **c-** Checkpoints

The images were processed in Agisoft PhotoScan, and the orthomosaic model is shown in figure (17-a), along with a zoomed-in crack section in figure (17-b).

Fig. (17): a-Orthomosaic of the street distresses obtained from a front position camera **b-**A zoomed-in crack section

Table (2) shows the accuracy check results of the check points. Figure (18) shows the model coordinates discrepancy versus depth.

Table (2): Accuracy check for street distresses captured via a front position camera

	Directly measured coordinates (m)		Model coordinates (m)		Discrepancies	
Point	X	Y	X	Y	e_X	e_Y
1	-6.38	1.53	-6.39	1.52	0.01	0.01
2	-3.77	6.52	-3.83	6.53	0.06	0.01
3	-2.53	11.82	-2.63	11.83	0.1	0.01
4	-3.41	22.91	-3.5	22.95	0.09	0.04
RMSE of X = 0.074m						
RMSE of Y = 0.022m						

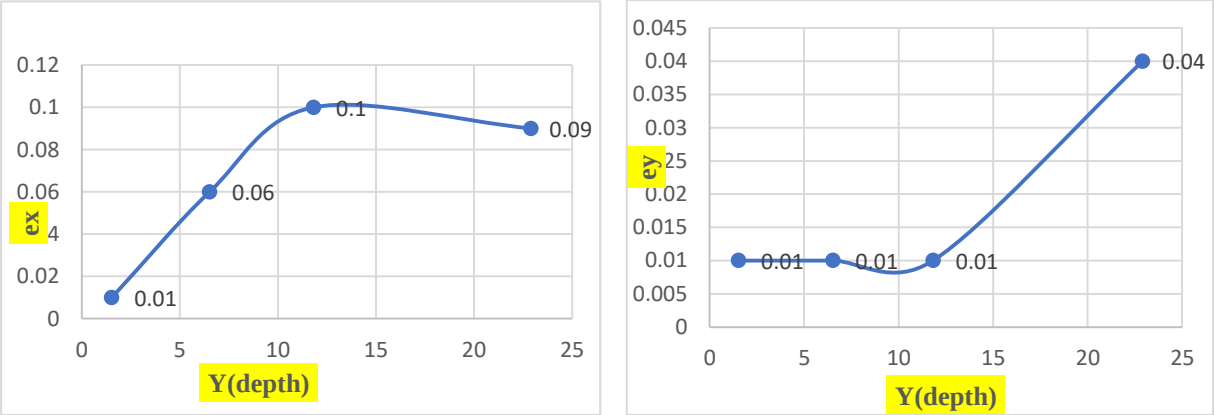

Fig.(18): Checkpoints coordinates versus depth of front position camera test

The results show that accepted accuracy in the Y coordinate was obtained for the first 15m of the test, while lower accuracy was noticed for X coordinates.

In the side-looking and front-looking mobile camera-based tests, the streets that were under study were almost level with little variation in heights, which didn't affect the camera height in a significant way. Both of the tests were used to create a 3-D orthomosaic model where the side looking-camera test required two passes to generate images, while the front-looking camera test required only one pass to generate these overlap images.

5. CONCLUSION

To obtain an efficient closed range model of the pavement surface, stereoscopic cameras are usually used, where two cameras are mounted on a bar in fixed positions. The exposure is made simultaneously by the synchronization of the shutters.

This study's unavailability of these stereometric cameras led to a different approach: moving the camera along the vehicle with its axis perpendicular to the movement direction and having the exposure performed in two passes. One pass is when the camera axis is tilted to the left of the vertical, and the second pass is when the camera axis is tilted to the right.

A second approach was also tested by mounting the camera in front of the moving vehicle and obtaining the stereoscopic coverage by forwarding overlapped images.

The spacing of the camera axis is an essential parameter to be studied carefully; otherwise, a gap will be observed in the model. The challenge is to find the best geometry combined with the vehicle speed and shutter speed to obtain a sufficient and uniform overlap. In using vertical close-range photogrammetry, this problem does not exist.

The indoor test experiments revealed the best parameters for pavement modeling and improving accuracy.

A slightly higher geometrical accuracy was obtained when increasing the angle of tilt and the height of the cameras.

A RMSE of ±0.013m and ±0.016m in X and Y checkpoints were obtained for 110° tilt angle and 1.5m camera height.

A RMSE of ±0.009m and ±0.013m in X and Y checkpoints were obtained for 115° tilt angle and 2.0m camera height.

Promising results and a satisfactory model were obtained in the front position camera as

one set of photos taken in one pass on the direction of travel is needed.

Shadows and tree coverage were a big problem to be tackled in further studies.

The control points measuring process was vital in this study. However, these points were primarily measured manually. That was a time-consuming process with moderate accuracy. A GPS attached to the imaging system might solve this problem for future recommendations.

Overall, the level of accuracy obtained in all of the tests complies with the expected accuracy, and the objectives of detecting each crack shape and position were successfully acquired and defined in the orthomosaic models obtained from each test.

REFERENCES

Abdulrahman, F. H., Kattan, R. A., & GILYANA, S. M. (2020). A Comparison between Unmanned Aerial Vehicle and Aerial Survey Acquired in Separate Dates for the Production of Orthophotos. *Journal of Duhok University, 23*(2), 52-66.

Ahmed, M., Haas, C., & Haas, R. (2011). Toward low-cost 3D automatic pavement distress surveying: the close range photogrammetry approach. *Canadian Journal of Civil Engineering, 38*(12), 1301-1313.

Cross, C., Farhadmanesh, M., & Rashidi, A. (2020). *Assessing Close-Range Photogrammetry as an Alternative for LiDAR Technology at UDOT Divisions*. Retrieved from

Fawzy, H. E.-D., Basha, A. M., & Botross, M. N. (2020). Estimating a mathematical formula of soil erosion under the effect of rainfall simulation by digital close range photogrammetry technique. *Alexandria Engineering Journal, 59*(6), 5079-5097.

Kattan, R., Abdulrahman, F. H., Gilyana, S. M., & Zaya, Y. Y. (2021). 3-D modelling and visualization of large building using photogrammetric approach. *Journal of Engineering Research*.

Knyaz, V., & Chibunichev, A. (2016). PHOTOGRAMMETRIC TECHNIQUES FOR ROAD SURFACE ANALYSIS. *ISPRS - International Archives of the Photogrammetry, Remote Sensing and Spatial Information Sciences, XLI-B5*, 515-520. doi:10.5194/isprs-archives-XLI-B5-515-2016

Lee, E. (2001). Geomorphological mapping. *Geological Society, London, Engineering Geology Special Publications, 18*(1), 53-56.

Martínez-Carricondo, P., Agüera-Vega, F., Carvajal-Ramírez, F., Mesas-Carrascosa, F.-J., García-Ferrer, A., & Pérez-Porras, F.-J. (2018). Assessment of UAV-photogrammetric mapping accuracy based on variation of ground control points. *International journal of applied earth observation and geoinformation, 72*, 1-10.

Roberts, J., Koeser, A., Abd-Elrahman, A., Wilkinson, B., Hansen, G., Landry, S., & Perez, A. (2019). Mobile terrestrial photogrammetry for street tree mapping and measurements. *Forests, 10*(8), 701.

Vosselman, G., & Maas, H.-G. (2010). *Airborne and terrestrial laser scanning*: CRC press.

Wolf, B. D. (2021). Ground Control Point Assessment for sUAS-based SfM Photogrammetry.

Yu, J. J., Kim, D. W., Lee, E. J., & Son, S. W. (2020). Determining the optimal number of ground control points for varying study sites through accuracy evaluation of unmanned aerial system-based 3D point clouds and digital surface models. *Drones, 4*(3), 49.